ACS OMEGA

http://pubs.acs.org/journal/acsodf

Article

Numerical Simulation on the Hydrogen Storage Performance of Magnesium Hydrogen Storage Reactors

Weishu Wang, Mengyao Zhang, Weihui Xu,* Boyan Tian, Renjie Li, Mengyuan Shang, and Zikun Yao

Cite This: *ACS Omega* 2023, 8, 4586−4596

Read Online

ACCESS | Metrics & More | Article Recommendations

ABSTRACT: Magnesium hydride (MH) is one of the most promising hydrogen storage materials. Under the hydrogen storage process, it will emit a large amount of heat, which limits the efficiency of the hydrogen storage reaction. In this paper, the hydrogen storage performance of the magnesium hydrogen storage reactor (MHSR) and the effect of structural parameters were studied by numerical simulation. The effect of different operating conditions on the hydrogen storage performance of the MHSR is analyzed. The volume energy storage rate (VESR) was taken as the comprehensive evaluation index (CEI). The results show that fins and heat exchange tubes can improve the heat transfer performance of the MHSR. Increasing fin thickness can reduce hydrogen storage time, but increasing fin spacing is the opposite. With the increase of fin thickness and fin spacing, VESR increases first and then decreases. With the increase of inlet temperature, the hydrogen storage time decreases first and then increases. When the inlet velocity is more than 5 m/s, the hydrogen storage time basically stays at 900 s. By optimizing the operating conditions, the hydrogen storage time can be shortened by 57.8%.

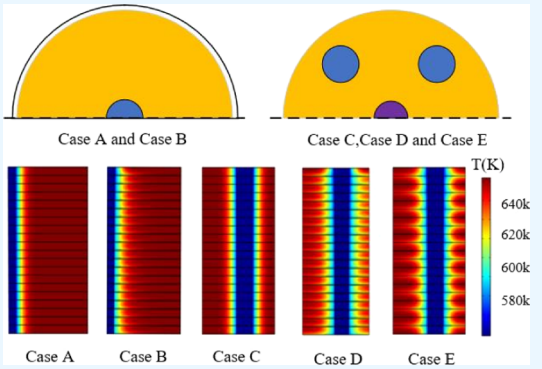

1. INTRODUCTION

With the development of industrialization, the consumption of fossil energy is increasing,[1,2] which causes a series of problems, such as exhaustion of traditional fossil energy, environmental pollution, and global warming.[3−5] Therefore, we urgently need to replace traditional fossil fuels with renewable energy.

Solar energy, wind energy, and hydrogen energy are the most common renewable energy sources at present. However, solar energy and wind energy have some shortcomings, such as intermittent and location-specific, which make them difficult to use on a large scale.[6,7] Hydrogen energy is an ideal energy carrier, which has the advantages of high efficiency, no pollution, high calorific value, and large-scale storage.[8] Nowadays, hydrogen energy has been successfully used as a propellant for aerospace and a fuel cell for vehicles.[9] The advantages and wide applications of hydrogen energy show that it is a promising future energy source. The key advantage of hydrogen fuel cell road vehicles is the intensive use in terms of driving range and load capacity.[10]

Technology for hydrogen storage is vital to the efficient and safe utilization of hydrogen fuel cell road vehicles.[11,12] The main hydrogen storage methods are high-pressure hydrogen storage, liquefaction hydrogen storage, and metal hydride hydrogen storage. Among them, metal hydride has attracted much attention because of its security and large storage capacity.[13] Hydrogen and metal elements undergo chemical adsorption reactions at a certain temperature and pressure to form compounds, so they have the ability to store hydrogen. The hydrogen storage capacity of hydrogen storage alloys is very strong; under the same temperature and pressure conditions, the density of hydrogen storage per unit volume is greater than that of liquefaction hydrogen storage.[14] Moreover, metal hydrides are solids, and there is no need for large, bulky cylinders required to store high-pressure hydrogen, nor extremely low temperature conditions such as liquid hydrogen.

Magnesium hydride (MH) has many advantages over other metal hydrogen storage materials, including large hydrogen storage capacity, abundant supply, low cost, and relatively good reversibility.[15,16] Due to the difficulty of recombination between hydrogen atoms and the surface layer of MH and the difficulty of dissociation between hydrogen molecules and magnesium surfaces, the reaction temperature and reaction speed of the hydrogen storage process are high, and the kinetic performance of hydrogen absorption and release is poor. The thermal environmental conditions of magnesium-based solid

Received: August 23, 2022
Accepted: December 30, 2022
Published: January 23, 2023

hydrogen storage limit its large-scale commercial development and application, so the heat dissipation design and optimization of the magnesium hydrogen storage reactor (MHSR) is crucial to the hydrogen storage performance.

Many studies on the heat and mass transfer properties of the MHSR have been carried out to deal with the temperature of the MHSR. Askri et al.[17] proposed a two-dimensional mathematical model of the hydrogen storage process in the MH reactor earlier, which provides a good foundation for analyzing the heat and mass transfer characteristics of the reactor. Nogita et al.[18] used in situ ultrahigh-voltage transmission electron microscopy (TEM) to directly verify the mechanisms of the hydride decomposition of bulk MgH_2 in Mg−Ni alloys and proved the hydriding/dehydriding mechanisms. Zhou et al.[19] investigated the growth characteristics of MgH_2 nanocrystallites to clarify the growth kinetics of MgH_2 crystallites. Chaise et al.[20] first designed a small MH tank, demonstrated the feasibility of hydrogen storage by MH, and then verified that the dense material consisting of MH and expanded graphite can better control the heat transfer in the tank. A study by Delhomme et al.[21] analyzed the performance of large hydrogen storage tanks by experiments and the properties of cycled composites. Garrier et al.[15] developed a mode for storing heat of the reaction with a phase-change material and tested it under various experimental conditions. Lutz et al.[22] developed a reactor that uses MH for hydrogen storage and magnesium hydroxide as a heat storage medium. The experimental study on the reactor shows that under a pressure of 1 MPa, hydrogen can be stored at high capacity. Limited by funds and equipment, many researchers utilize numerical methods to analyze the heat and mass transfer characteristics of the MHSR. Chaise et al.[23] proposed a criterion for allowing the flow of hydrogen to be ignored in numerical studies. Shen and Zhao[24] studied the effect of metal foam on heat and mass transfer in a metal hydrogen storage reactor, evaluated various factors affecting the reaction time, and analyzed the sensitivity. Gi et al.[25] synthesized various types of Nb oxides and mixed them with Mg, and their catalytic properties were investigated, and concluded that the chemical state of Nb is an important factor in catalyzing the desorption/absorption of hydrogen by Mg, and the catalytically active state can be preserved without further treatments. Zamengo et al.[28] used expanded graphite (EG) to enhance the thermal conductivity in the packed bed reactors of magnesium oxide/water (MgO/H_2O) chemical heat pumps (CHP), which demonstrated that the EM pellets had a higher reactivity than pure $Mg(OH)_2$ pellets because of their higher thermal conductivity. A study by Dong et al.[26] who analyzed the addition of 20 wt % ENG to MgH_2 is considered the best choice to increase the heat transfer performance of the reactor. The study of Poupin et al.[27] also showed that the thermal and cycling properties of the hydride material are enhanced by the addition of TiB_2 and exfoliated natural graphite. Based on numerical studies of the effects of compacts of metal hydride and metal fins in metal hydride reactors, Bao[29] took the gravimetric heat storage rate as the comprehensive evaluation index (CEI) of the reactor. To evaluate the overall performance of metal hydride reactors, Feng et al.[30] defined a comprehensive index that considered finite-material and finite-time constraints, as well as available output energy.

The above research involves the heat and mass transfer characteristics of magnesium-based solid hydrogen storage reactors. The research is carried out from the aspects of heat exchanger design and heat storage materials. There are few studies on the structural parameters and operating parameters of the reactor. Moreover, most scholars mainly focus on the hydrogen storage time, without paying attention to the change of energy density of the reactor. In this paper, the influence of the MHSR on hydrogen storage performance was studied by numerical simulation. The volume energy storage rate (VESR) was used as a CEI to determine the relative optimal structure of the reactor. The influence of different operating conditions on the hydrogen storage performance of the reactor was discussed, and the relative optimal operating conditions were obtained.

2. MAGNESIUM HYDROGEN STORAGE REACTOR

2.1. Physical Model of the MHSR. The essence of metal hydrogen storage is that metal reacts with hydrogen to generate metal hydride. The hydrogen storage reaction of metal is usually accompanied by energy conversion, which destroys the optimal temperature condition for metal hydrogenation. Therefore, the process of metal hydrogen storage needs a heat exchanger to ensure that the metal hydrogen storage material is in the best temperature state. The process of metal hydrogen storage is shown in Figure 1.

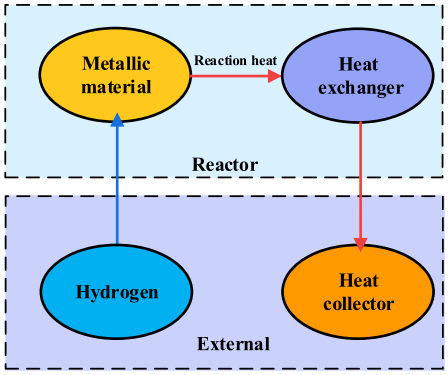

Figure 1. Process of metal hydrogen storage.

The chemical reaction of hydrogen absorption of MH is as follows:

$$Mg(s) + H_2(g) \rightarrow MgH_2(s) + \Delta H \quad (1)$$

whereΔH is the reaction enthalpy, −75 kJ/mol.[31,32]

Hydrogen reacts with metals at any temperature and pressure. The hydrogenation of magnesium is accompanied by intense exotherm. Heating will raise the temperature of magnesium, leading to the increase of equilibrium pressure, thus affecting the hydrogen storage rate. However, if the cooling capacity is too strong, the temperature of magnesium will be too low, which will also reduce the hydrogenation rate. Therefore, the temperature should be kept within a certain range.

To explore the influence of fin structure parameters on hydrogen storage performance, the existing efficient hydrogen storage model in this study is improved.[29] Figure 2 shows the five MHSRs with different means of heat transfer enhancement. The diameter of the MHSR is 209 mm, the diameter of the heat exchanger tube is 20 mm, and the diameter of the hydrogen supply channel is 18 mm. A synthetic oil (SCHULTZ S730) is used as heat transfer fluid (HTF) in the MHSR.

https://doi.org/10.1021/acsomega.2c03484
ACS Omega 2023, 8, 4586−4596

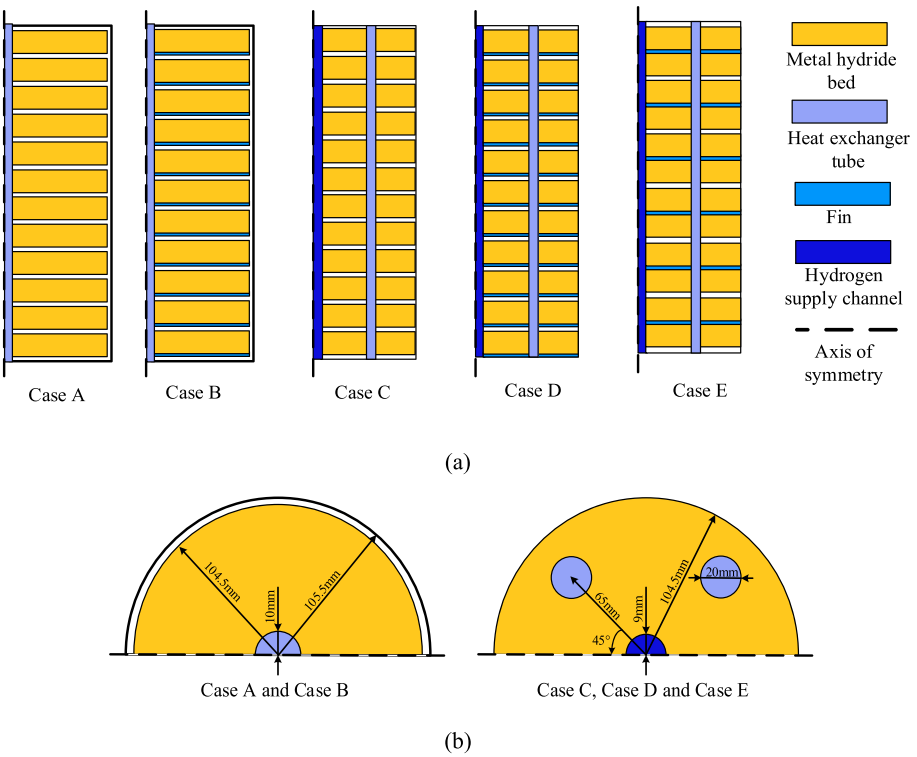

Figure 2. Schematic diagram of metal hydride reactors. (a) Front view. (b) Top view.

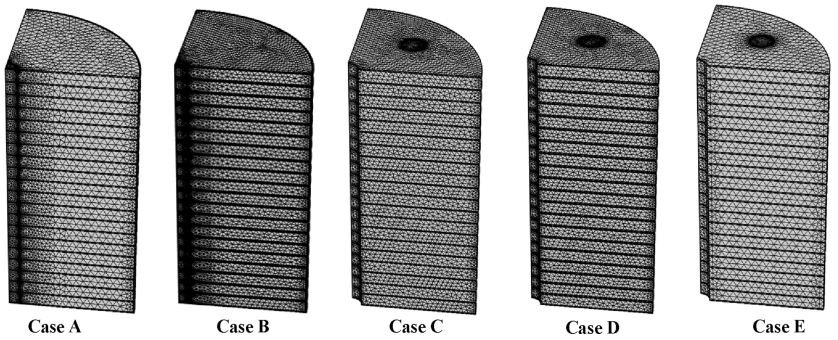

Figure 3. Mesh diagram of metal hydride reactors.

Case A: The heat exchange tube is placed in the center of the reactor. There is a space of 1 mm between the upper and lower MH reaction beds and 1 mm between the MH reaction bed and the reactor, and hydrogen flows in from the reactor wall.

Case B: The heat exchange tube is placed in the center of the reactor. There is a space of 1 mm above the reaction bed and 1 mm between the MH reaction bed and the reactor, the fins are placed under the metal hydride bed, and hydrogen flows in from the reactor wall.

Case C: The hydrogen supply channel is located in the center of the reactor, and four heat exchange tubes are symmetrically placed in the reactor. There is a space of 1 mm between the upper and lower MH reaction beds.

Case D: The hydrogen supply channel is located in the center of the reactor, four heat exchange tubes are symmetrically placed in the reactor, the fins are placed under the MH reaction bed, and a space of 1 mm is left above the metal hydride bed.

Case E: The hydrogen supply channel is located in the center of the reactor, four heat exchange tubes are symmetrically placed in the reactor, every two metal hydride beds are a group, fins are placed in the middle of each group, and 1 mm spaces are left above and below each group.

Because five MHSRs are all symmetric structures, to improve the calculation efficiency, a quarter of the physical model is selected as the numerical solution area. The heat exchange tubes, fins, and hydrogen supply channels are encrypted locally. The mesh models are shown in Figure 3.

2.2. Performance Assessment. Hydrogen storage time is an important index for evaluating the MHSR. However, with the development of hydrogen storage technology and the application of metal hydrogen storage in automobiles, the energy density of the MHSR is becoming more and more important. Although the measures to enhance the heat transfer capacity of the reactor can reduce the hydrogen storage time, they will reduce the energy density of the reactor. Therefore, the VESR is used for the CEI of the reactor. The VESR can be expressed as follows:

https://doi.org/10.1021/acsomega.2c03484
ACS Omega 2023, 8, 4586−4596

$$G = mq\frac{wt(X_d - X_0)}{Vt_d} \quad (2)$$

where m is the quality of the metal hydride bed, kg; V is the volume of the MHSR, m^3; t is the hydrogen storage time, s (it is considered that the reaction is finished when the reaction fraction is 0.95); wt is the maximum mass content of hydrogen in the MH; and q is the calorific value of hydrogen, 120 kJ/mol.

3. MATHEMATICAL MODEL

3.1. Assumptions.

(1) The local thermal equilibrium is valid for the MHB and hydrogen.
(2) Ignoring radiation heat transfer of particles in the MHB.[32−36]
(3) The thermophysical properties of the MHB and HTF are constant during hydrogen storage.
(4) Hydrogen is considered to be an ideal gas.
(5) Because the resistance in free space is much less than that in the MHB, the flow in free space is ignored.

3.2. Governing Equations. *3.2.1. Magnesium Hydride Bed.* MHB as a porous medium is the main structure for hydrogen storage. Therefore, the hydrogen flow within the MH bed can be expressed by Darcy's law, and the effective parameters of porous media can be solved by the volume average method. The governing equations for heat and mass transfer in the MH bed are shown below.

Continuity equation:

$$\varepsilon\frac{\partial\rho_g}{\partial t} + \nabla\cdot(\rho_g u_g) = -Q_m \quad (3)$$

Darcy's law:

$$u_g = -\frac{\kappa}{\mu}\nabla p_g \quad (4)$$

Energy equation:

$$\rho_{eff}c_{eff}\frac{\partial T}{\partial t} + \rho_{eff}c_{eff}u_g\cdot\nabla T = \lambda_{eff}\nabla^2 T + \frac{Q_m}{M_g}\cdot\Delta H \quad (5)$$

$$Q_m = \frac{\rho_s wt(1-\varepsilon)}{M_g}\frac{dX}{dt} \quad (6)$$

$$\rho_{eff} = (1-\varepsilon)\rho_s + \varepsilon\rho_g \quad (7)$$

$$c_{eff} = (1-\varepsilon)c_s + \varepsilon c_g \quad (8)$$

$$\lambda_{eff} = (1-\varepsilon)\lambda_s + \varepsilon\lambda_g \quad (9)$$

where ρ is the density, kg/m^3; c is the specific heat capacity, s; T is the temperature, K; p is the pressure, MPa ; u is the velocity, m/s; μ is the dynamic viscosity, Pa·s; λ is the thermal conductivity, W/(m·K); ε is the porosity of MHB; κ is the permeability of MHB, m^2; Q_m is the hydrogen absorbed per unit time per unit volume, $g/(m^3\cdot s)$; wt is the maximum mass content of hydrogen in the MH; M is the molecular weight; X is the reacted fraction; and the subscripts eff, s, and g are the effective coefficient, MHB, and hydrogen, respectively.

The equilibrium pressure is determined by the van't Hoff equation as follows:

$$\ln\left(\frac{P_{eq}}{P_{ref}}\right) = \frac{\Delta H}{R_g T} - \frac{S_g}{R_g} \quad (10)$$

The kinetic equation of hydrogen absorption of the MHB is as follows:[23]

$$\frac{dX}{dt} = C_a e^{-E_a/R_g T}\ln\left(\frac{P_g}{P_{eq}}\right)(1-X) \quad (11)$$

where P_{eq} is the equilibrium pressure, MPa; P_{ref} is the reference pressure, 0.1 MPa; ΔH is the enthalpy of the absorption reaction, kJ/mol; S_g is the entropy of the absorption reaction, $J\cdot mol^{-1}\cdot K^{-1}$; R_g is the gas constant, 8.314 J/(mol K); C_a is the Arrhenius parameter for absorption, s^{-1}; E_a is the activation energy for absorption, J/mol.

3.2.2. Heat Exchanger Tubes and Fins. The addition of a finned tube heat exchanger is an important means to improve the heat transfer performance of the MHSR. Heat exchange tubes and fins are the main heat exchanger of the MHSR. The HTF flows in the heat exchange tube to heat dissipation for the MHB. Because of the thin wall thickness and high thermal conductivity of the heat exchange tubes, the heat conduction of the pipe wall can be neglected. The heat and mass transfer equations of the heat exchanger are as follows:

Continuity equation:

$$\rho_f\nabla\cdot u_f = 0 \quad (12)$$

Momentum equation:

$$\rho_f\frac{\partial u_f}{\partial t} + \rho_f(u_f\cdot\nabla u_f) = \nabla\cdot[\mu_f(\nabla u_f + (\nabla u_f)^T)] - \nabla p_f \quad (13)$$

Energy equation for the HTF:[27]

$$\rho_f c_f\frac{\partial T}{\partial t} + c_f\rho_f u_f\nabla T = \lambda_f\nabla^2 T \quad (14)$$

Energy equation for the fin:[30]

$$\rho_{fin}c_{fin}\frac{\partial T}{\partial t} = \lambda_{fin}\nabla^2 T \quad (15)$$

where the subscripts f and fin are the HTF and fin, respectively.

3.3. Simulation Parameters. The numerical simulation in this paper is done by using COMSOL Multiphysics software. COMSOL Multiphysics software has been widely used in chemical reactions, fluid dynamics, fuel cells, thermal conductivity, porous media, and other fields.

3.3.1. Initial and Boundary Conditions. The reaction fraction of the MH reaction bed and the hydrogen pressure in the reactor were 0.001 and 0.1 MPa at the beginning; radiant heat transfer in the reactor was ignored; synthetic oil (SCHULTZ S730) was used as the cooling medium. The initial temperature of the reaction bed is the inlet temperature of the cooling medium. The outer surface of the reactor is set to an adiabatic surface. The thermophysical properties of the material remain unchanged during hydrogen storage.

3.3.2. Thermophysical Properties. The thermophysical properties used for this study are listed in Table 1.

3.3.3. Mode Validation. To ensure that different mesh sizes do not affect the numerical results, the mesh independency checks are conducted about the hydrogen storage performance of the MHSR. It is shown in Figure 4 that when the number of meshes is 800,000 cells, the influence of the number of cells on

https://doi.org/10.1021/acsomega.2c03484
ACS Omega 2023, 8, 4586−4596

Table 1. Thermophysical Properties of Materials[17,23]

parameter	value
density of MHB, HTF, and fin	1800, 730, and 2700 kg/m^3
effective thermal conductivity of MHB, HTF, and fin	4.2 (radial)/1.0 (axial), 0.0937, and 201 W/(m·K)
specific heat of MHB, HTF, and fin	1545, 2530, and 900 J/(kg K)
dynamic viscosity of HTF	2.4×10^{-4} Pa s
porosity of MHB	0.31
permeability of MHB	5.9×10^{-16} m^2
Arrhenius parameter for absorption	2.9×10^{8} s^{-1}
activation energy for absorption	130 kJ/mol
enthalpy of the absorption reaction	−75 kJ/mol
entropy of the absorption reaction	−135.6
maximum mass content of hydrogen in the MH	6%

the numerical results is negligible. Therefore, all numerical simulation cases in this study use mesh more than 800,748 cells.

Model validation was performed using Chaise et al.'s[23] experimental data. Figure 5 shows the comparison of the simulation results and the experimental data. The broken lines in the figure are the numerical results, and the solid lines in the figure are the experimental results. As can be seen from the figure, the simulation results of the temperature and reaction fraction coincide with the experimental results within the error range. Therefore, it also fully shows that under reasonable assumptions and simplified conditions, numerical simulation can replace the experimental study of the MHSR.

4. RESULTS AND DISCUSSION

4.1. Comparison of Characteristics in Five Different MHSRs. Figure 6 shows the temperature field of five different MHSRs at 1500 s. Under the same operating conditions, five different MHSRs were simulated, in which the hydrogen supply pressure and initial temperatures of MHBs and HTF were 1.2 MPa, 570 K, and 570 K, respectively. Because the hydrogen storage reaction gives off a lot of heat, most of the MHBs are about 650 K. As can be seen from Figure 6, regardless of how the position of the heat exchange tube and the fin structure change, the lower temperatures are distributed near the heat exchange tubes and fins, indicating that a stronger cooling effect is produced at these locations. The temperature gradually increases from the center of the heat exchange tube to both sides until it is stable, there is a clear transition zone in the middle, the width of the transition zone of case B is greater than that of case A, and the width of the transition zone of case D and case E is greater than that of case C, indicating that the presence of fins increases the thermal conductivity of the reactor and makes its temperature distribution more uniform. The above conclusions show that the addition of fins and heat exchange tubes can greatly improve the heat transfer performance of magnesium-based solid hydrogen storage reactors.

Figure 7a shows the comparison of performance in five different MHSRs. The hydrogen storage time from less to more is case D, case E, case B, case C, and case A, respectively. This is because the more uneven the temperature distribution of the MHSR, the more areas in the high-temperature environment and the worse its heat dissipation performance, resulting in a smaller reaction speed of the hydrogenation reaction and an increase in hydrogen storage time. This shows that adding heat exchangers and fins can effectively shorten the hydrogen storage time of the MHSR.

Figure 7b shows the VESR of five different MHSRs. Although the hydrogen storage time of case B (11,125 s) is 20% less than the hydrogen storage time of case C (13,916 s), the VESR of case B (765 kW/m^3) is 14.5% less than the VESR of casee C (895 kW/m^3). This is because although the heat transfer performance of the MHSR is enhanced by increasing the fins, this measure introduces additional volume, and the superposition of the two effects together leads to a decrease in the VESR of the reactor. This shows that in the structural changes of the MHSR, the number of fins cannot be increased blindly. Among the five cases, case D has the largest VESR, which is 3165 kW/m^3. Therefore, considering the hydrogen storage time and energy density, case D is the best MHSR in the five cases. The following discussion will be for the MHSR in case D.

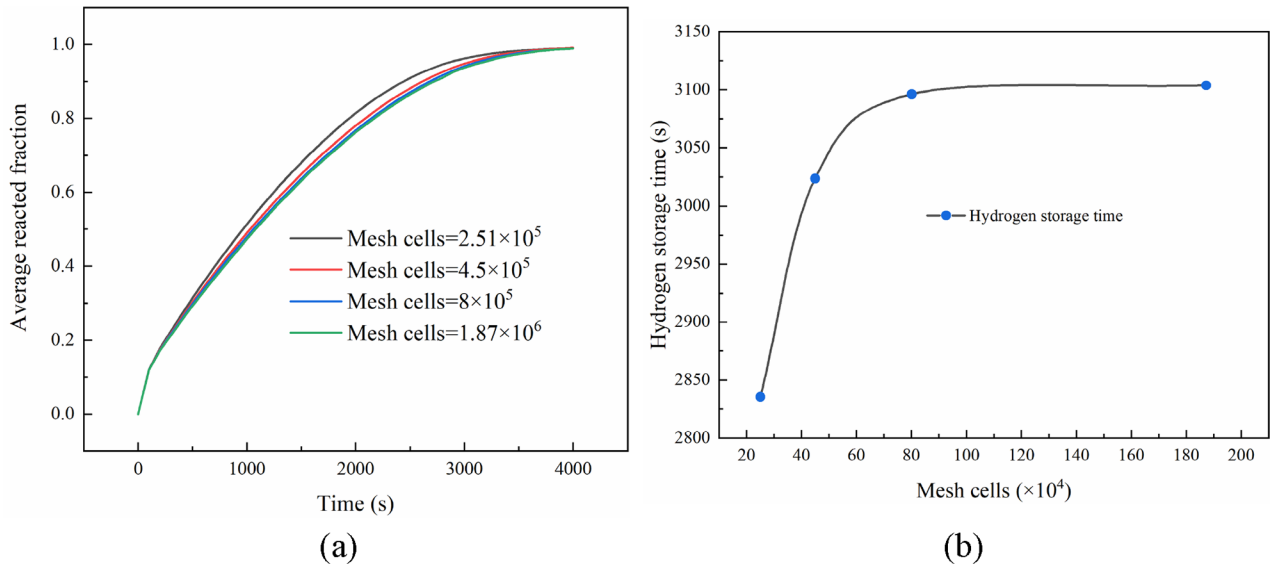

Figure 4. Mesh independent. (a) Average reacted fraction. (b) Hydrogen storage time.

https://doi.org/10.1021/acsomega.2c03484
ACS Omega 2023, 8, 4586−4596

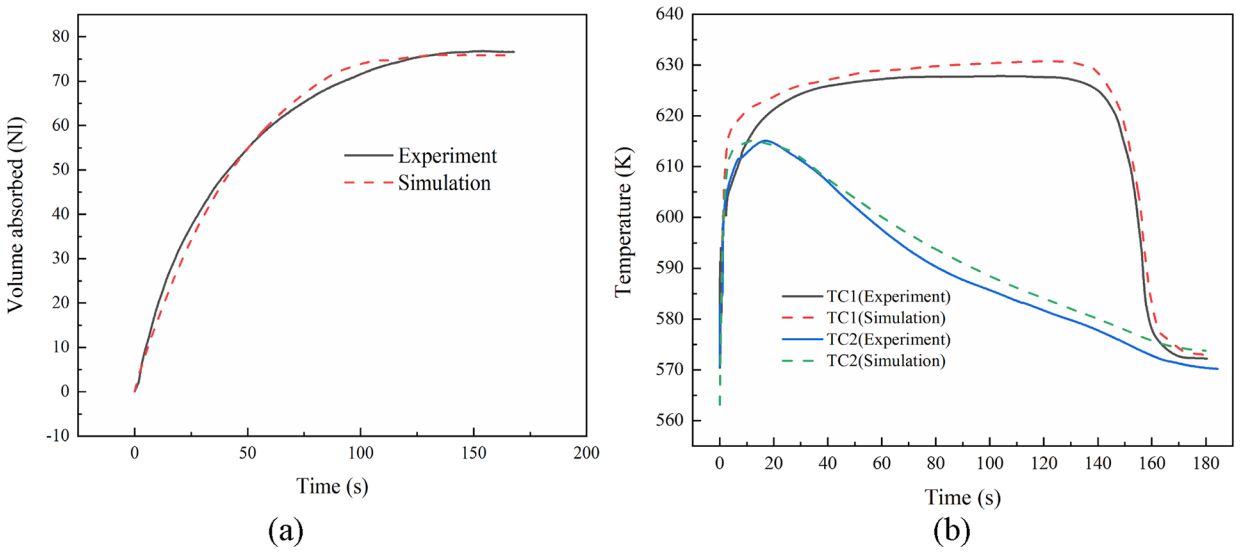

Figure 5. Comparison of the simulation results and the experimental data. (a) Average reacted fraction. (b) Temperature.

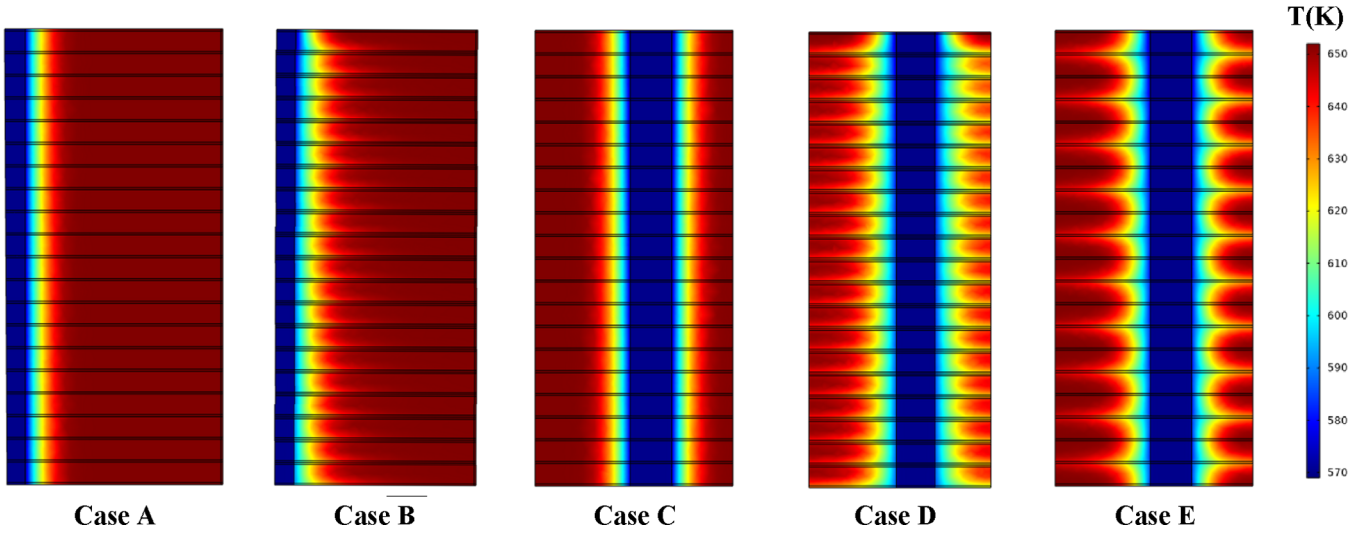

Figure 6. Comparison of the temperature field in five different MHSRs.

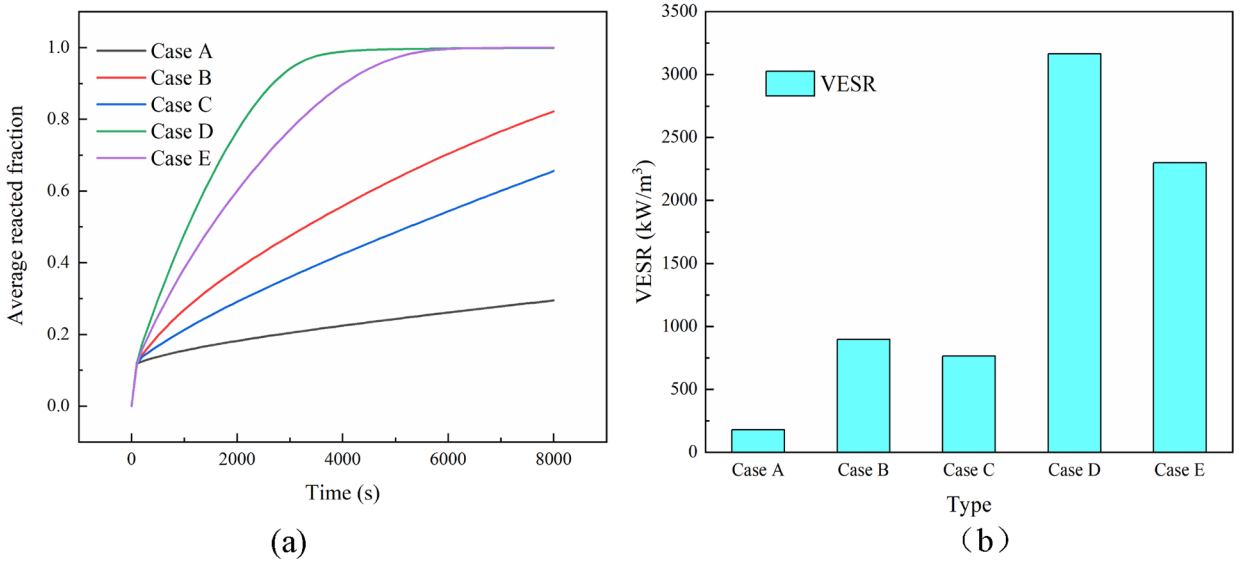

Figure 7. Comparison of performance in five different MHSRs. (a) Average reacted fraction. (b) VESR.

https://doi.org/10.1021/acsomega.2c03484
ACS Omega 2023, 8, 4586−4596

Figure 8 shows the temperature changes of the three locations of MHB with time. The temperature of the three

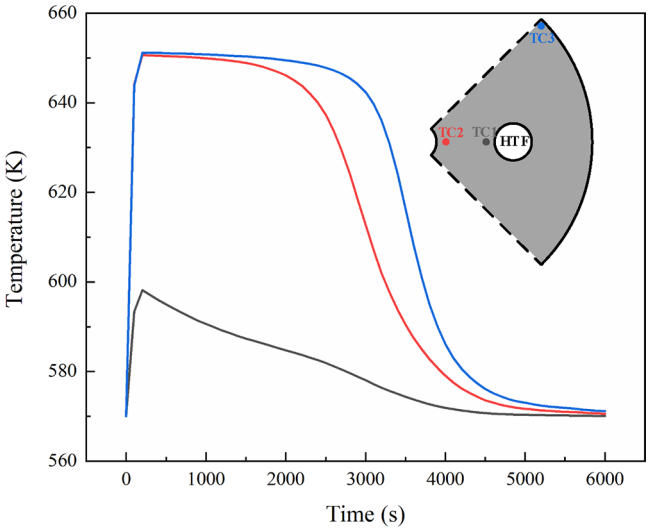

Figure 8. Time evolution of temperature at three positions of the MHB.

points increases rapidly in the first 200 s. This means that the hydrogen storage reaction releases a large amount of reaction heat. Also, the farther away from the heat exchanger tube, the higher the temperature rise, and the longer the high temperature state is maintained. This is because the farther away from the heat exchange tube, the worse the heat dissipation capacity, and the heat generated by the hydrogen storage reaction is not yet absorbed by the bed, which will make the place in a higher-temperature environment for a long time and the reaction rate become smaller.

Figure 9 shows the distribution of reaction parts in the MHB at different times. Hydrogen storage first occurs near HTF, and with the increase of time, it spreads around with HTF as the center, and finally reaches an equilibrium state.

4.2. Effects of the Structure of the MHSR. Adding fins is a common measure to enhance heat transfer, but adding fins will inevitably increase the volume and reduce the energy density of the MHSR. Fin thickness and fin pitch are the main factors influencing the heat transfer enhancement effect of fins, and their changes will affect the hydrogen storage performance of the whole MHSR.

Figure 10 shows the influence of the fin thickness on the hydrogen storage performance of the MHSR. The hydrogen storage time of the reactor with a fin thickness of 1 mm is quite different from that of the reactors with the fin thickness of 2, 3, and 4 mm, and the hydrogen storage times are 3096, 2339, 2151, and 2131 s, respectively. With the increase of fin thickness from 1 to 4 mm, the hydrogen storage time decreases but the extent of hydrogen storage time decreases is smaller. With the increase of fin thickness, the VESR increases first and then decreases. When the thickness of the fins is from 2 to 3 mm, the VESR changes little. The reasonable value of fin thickness in this study is about 2.5 mm.

Figure 11 shows the influence of fin pitch of the MHSR on hydrogen storage performance. The storage times of the fin pitch of 9, 11, and 13 mm are 2063, 2210, and 2332 s, respectively. With the fin pitch increasing from 9 to 13 mm, the hydrogen storage time increases. Due to the increase of fin pitch, the number of fins in the reactor with the same length decreases, which weakens the heat transfer effect. With the increase of fin pitch, the VESR first increases and then decreases. The maximum VESR occurs between 9 and 10 mm fin pitch. In this study, to improve the energy density of the MHSR as much as possible, the selected fin pitch is 10 mm.

4.3. Effects of Operating Conditions on the MHSR. Operating conditions such as hydrogen supply pressure, inlet temperature of HTF, and inlet velocity of HTF are the key factors for the hydrogen storage performance of the MHSR. The optimal operating conditions are different for different MHSRs.

Figure 12 shows the effects of the hydrogen supply pressure on the hydrogen storage performance of the MHSR. The hydrogen storage time of the MHSR increases with the increase of hydrogen supply pressure. The reaction fraction increased with time, and the hydrogen storage rate decreased with time. The initial reaction rate of hydrogenation is extremely fast, and the higher the hydrogen supply pressure, the faster the initial reaction rate of hydrogenation. This means that the higher the hydrogen supply pressure is, the higher the average temperature of the MHB in the initial stage of

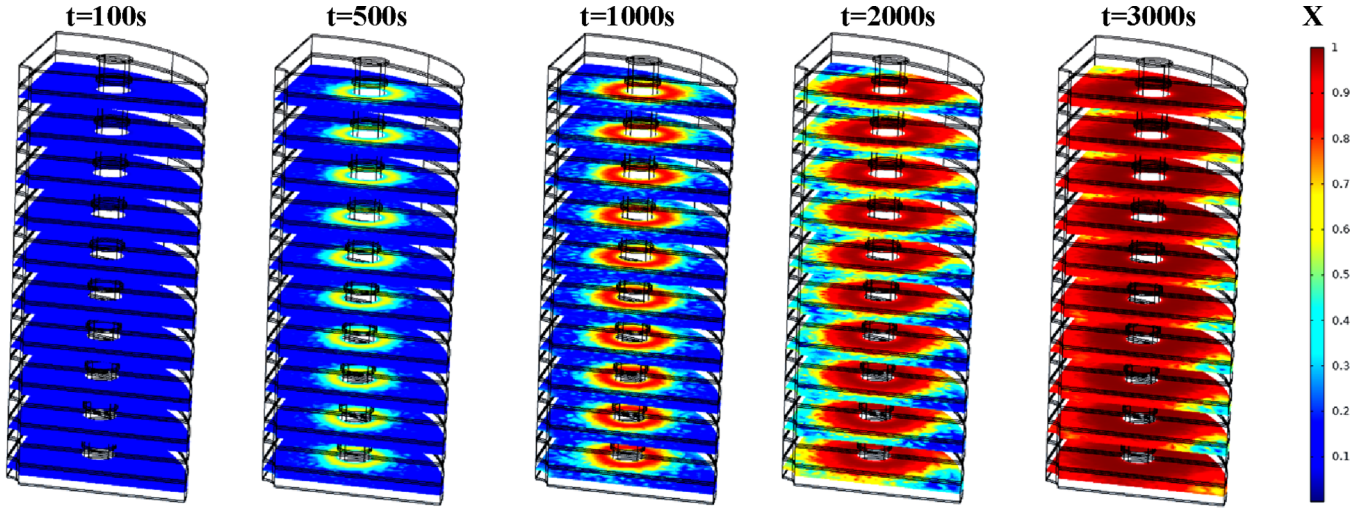

Figure 9. Distribution of the reacted fraction in the MHB at different times.

https://doi.org/10.1021/acsomega.2c03484
ACS Omega 2023, 8, 4586−4596

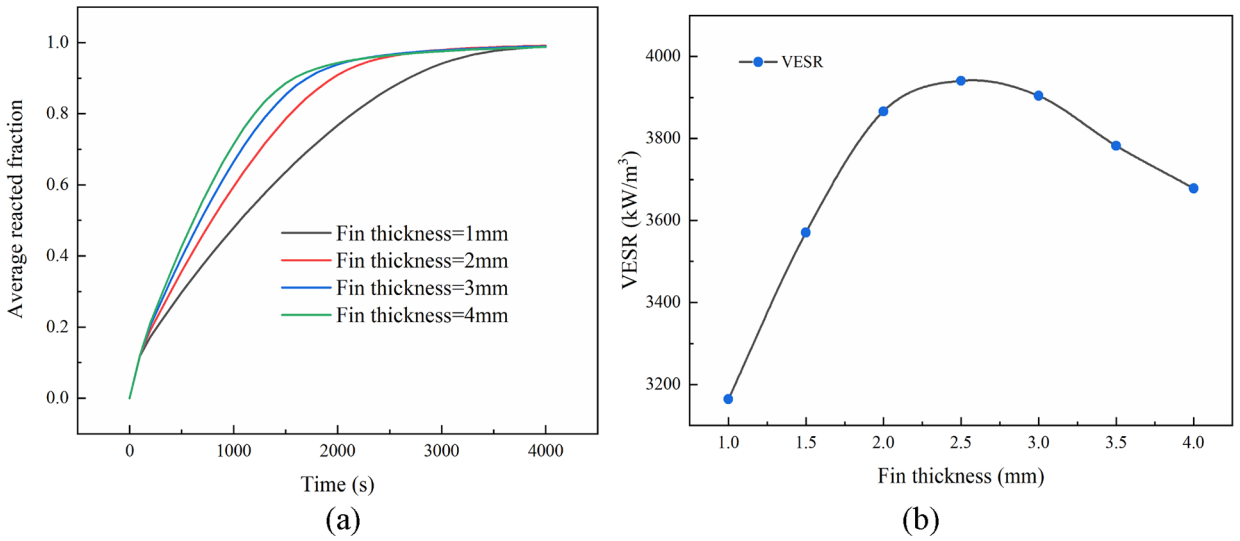

Figure 10. Fin thickness on hydrogen storage performance. (a) Average reacted fraction. (b) VESR.

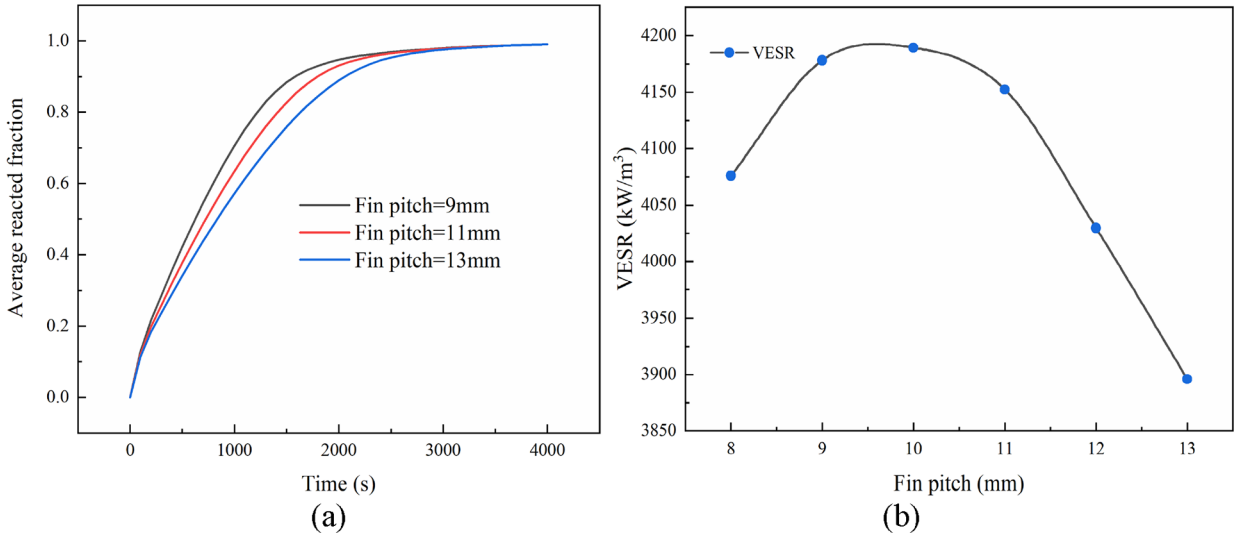

Figure 11. Fin spacing on hydrogen storage performance. (a) Average reacted fraction. (b) VESR.

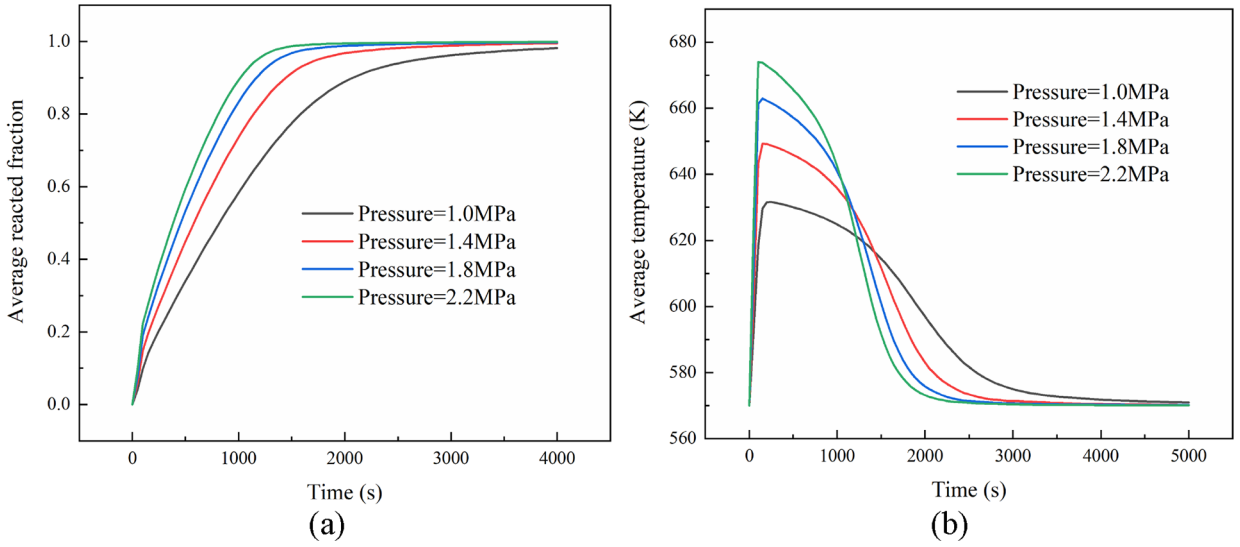

Figure 12. Hydrogen supply pressure on hydrogen storage performance. (a) Average reacted fraction. (b) Average temperature.

https://doi.org/10.1021/acsomega.2c03484
ACS Omega 2023, 8, 4586−4596

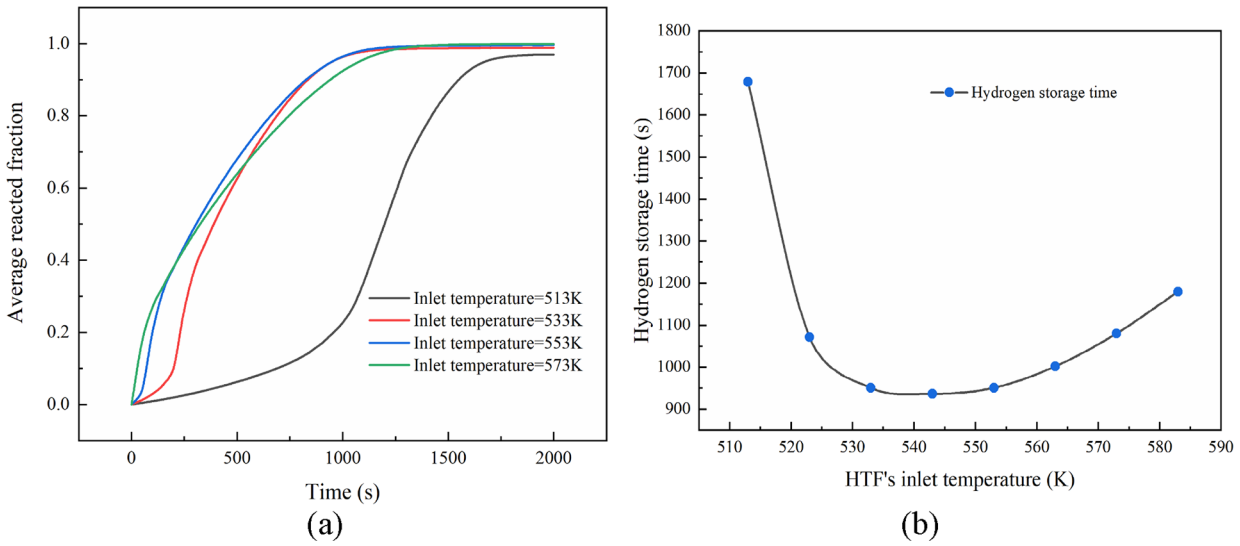

Figure 13. Inlet temperature of HTF on hydrogen storage performance. (a) Average reacted fraction. (b) Hydrogen storage time.

hydrogenation is. This is because MH will be sintered at a temperature higher than 703 K, which hinders hydrogenation and reduces the hydrogen storage density of the reactor.[37,38] According to the previous discussion in this paper, the maximum temperature of the MHB will reach the equilibrium temperature corresponding to the hydrogen supply pressure. Therefore, the maximum temperature of the MHB is limited to 700 K, and the equilibrium pressure corresponds to the temperature based on eq 10, which is 3 MPa. The optimal hydrogen supply pressure of the MHSR in this study is 3 MPa.

Figure 13 shows the influence curves of HTF inlet temperature on the hydrogen storage performance of the MHSR. In the initial stage of the reaction, the higher the HTF inlet temperature, the faster the reaction rate. However, with the progress of the reaction, the reaction rate at an HTF inlet temperature of 573 K is gradually slower than that at the HTF inlet temperatures of 553 and 533 K. This phenomenon can be explained as follows: the higher the inlet temperature of the HTF, the faster the MHB reaches the optimum temperature of the MHSR. With the reaction process, the temperature of the MHB will rise, and part of the MHB will be in equilibrium. The higher the inlet temperature of the HTF, the worse the heat dissipation capacity, and the longer the MHB is in an equilibrium, which hinders the reaction. With the increase of temperature, the reaction rate first increases and then decreases. This is because the heat released at the beginning of the reaction will promote the reaction, but the reaction rate reaches the maximum value when it reaches a certain level, and then starts to decrease under the influence of equilibrium pressure. At a certain pressure, the reaction rate of the hydrogenation reaction increases and then decreases with the change of temperature, but the fuel temperature is too low to cause the reaction to reach the optimal temperature. So when the inlet temperature is 513 K, the heat dissipation capacity is larger than the heat release capacity. As the reaction reaches equilibrium, the reaction rate still does not reach the maximum value, so the curve shows different situations. The hydrogen storage time first decreases and then increases with the inlet temperature of HTF. The hydrogen storage time is almost constant when the inlet temperature of HTF is between 533 and 553 K. Therefore, to reduce the heat dissipation pressure and prevent the MHB temperature from rising rapidly, the optimal HTF inlet temperature of the MHSR is 533 K.

Figure 14 shows the curve of the influence of HTF inlet velocity on the hydrogen storage time of the MHSR. It can be

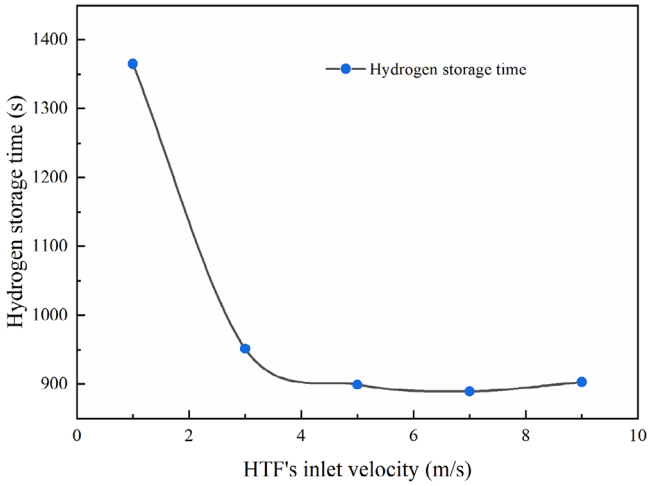

Figure 14. Inlet velocity of HTF on the hydrogen storage time of the MHSR.

clearly seen from the figures that the inlet velocity of the HTF increases from 1 to 5 m/s, and the hydrogen storage time is reduced by 466 s. The inlet velocity of the HTF ranges from 5 to 9 m/s, and the hydrogen storage time is nearly the same, all around 900 s. As the inlet velocity of the HTF increases, the power of the pump will inevitably increase, so the optimal inlet velocity of the HTF is 5 m/s.

Figure 15 compares the variation of average reaction fraction with time under the optimal and initial operating conditions. The optimum operating conditions are as follows: the hydrogen supply pressure, inlet temperature, and inlet velocity of the HTF are 3 MPa, 533 K, and 5 m/s, respectively. The initial operating conditions are as follows: the hydrogen supply pressure, inlet temperature, and inlet velocity of the HTF are 1.2 MPa, 570 K, and 3 m/s, respectively. The hydrogen storage reaction rate under the optimum operation conditions is more stable than that under the initial conditions. The hydrogen

https://doi.org/10.1021/acsomega.2c03484
ACS Omega 2023, 8, 4586−4596

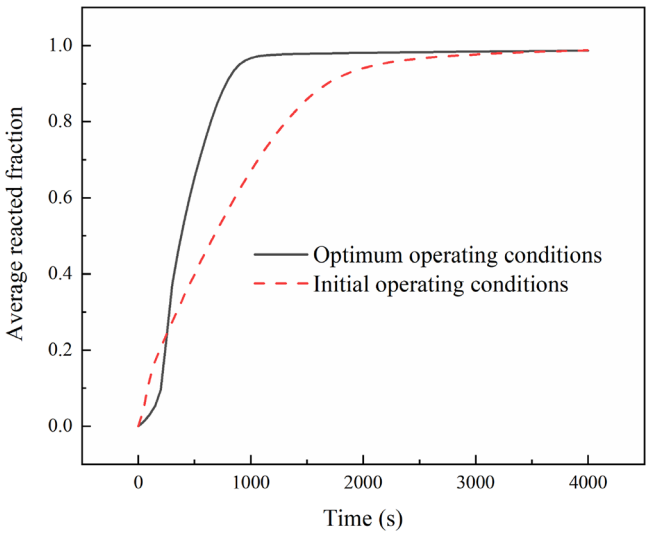

Figure 15. Comparison of optimum and initial operating conditions.

storage time (899 s) under the optimal conditions is 57.8% shorter than that under the initial conditions (2129 s). It shows that the operating conditions have an important influence on the hydrogen storage performance of the MHSR.

5. CONCLUSIONS

The structure characteristics of the MHSR and operation conditions are discussed in this paper. For MHSR performance, the VESR is used as the CEI. The following main results are obtained:

1) Increasing the number of fins and heat exchange tubes can greatly improve the heat transfer performance of the MHSR, but introducing extra volume will reduce the VESR.
2) With the increase of fin thickness, the hydrogen storage time decreases gradually, while the VESR increases first and then decreases.
3) The hydrogen storage time increases with the increase of fin spacing and hydrogen supply pressure, while the VESR increases first and then decreases.
4) With the increase of inlet temperature, the hydrogen storage time first decreases and then increases. When the inlet temperature of HTF is between 533 and 553 K, the hydrogen storage time is almost constant.
5) The hydrogen storage time decreases with the increase of the inlet velocity. When the inlet velocity is more than 5 m/s, the hydrogen storage time basically stays at 900 s.

AUTHOR INFORMATION

Corresponding Author

Weihui Xu − *School of Electric Power, North China University of Water Resources and Electric Power, Zhengzhou, Henan 450045, P. R. China*; Email: xuweihui@ncwu.edu.cn

Authors

Weishu Wang − *School of Electric Power, North China University of Water Resources and Electric Power, Zhengzhou, Henan 450045, P. R. China*; orcid.org/0000-0001-7623-4047

Mengyao Zhang − *School of Electric Power, North China University of Water Resources and Electric Power, Zhengzhou, Henan 450045, P. R. China*

Boyan Tian − *School of Electric Power, North China University of Water Resources and Electric Power, Zhengzhou, Henan 450045, P. R. China*

Renjie Li − *School of Electric Power, North China University of Water Resources and Electric Power, Zhengzhou, Henan 450045, P. R. China*

Mengyuan Shang − *School of Electric Power, North China University of Water Resources and Electric Power, Zhengzhou, Henan 450045, P. R. China*; orcid.org/0000-0002-3283-120X

Zikun Yao − *School of Electric Power, North China University of Water Resources and Electric Power, Zhengzhou, Henan 450045, P. R. China*

Complete contact information is available at: https://pubs.acs.org/10.1021/acsomega.2c03484

Notes

The authors declare no competing financial interest.

ACKNOWLEDGMENTS

This work was supported by the Project of Central Plains Science and Technology Innovation Leading Talents of Henan Province under grant no. 224200510022.

REFERENCES

(1) Magazzino, C.; Mele, M.; Schneider, N. A Machine Learning approach on the relationship among solar and wind energy production, coal consumption, GDP, and CO_2 emissions. *Renewable Energy* **2021**, *167*, 99−115.

(2) Mellouli, S.; Askri, F.; Dhaou, H.; Jemni, A.; Ben Nasrallah, S. Numerical simulation of heat and mass transfer in metal hydride hydrogen storage tanks for fuel cell vehicles. *Int. J. Hydrogen Energy* **2010**, *35*, 1693−1705.

(3) Mallick, D.; Mahanta, P.; Moholkar, V. S. Synergistic effects in gasification of coal/biomass blends: analysis and review. *Coal Biomass Gasif.* **2018**, 473−497.

(4) Martins, F.; Felgueiras, C.; Smitkova, M.; Caetano, N. Analysis of fossil fuel energy consumption and environmental impacts in European countries. *Energies* **2019**, *12*, 964.

(5) Shindell, D.; Smith, C. J. Climate and air-quality benefits of a realistic phase-out of fossil fuels. *Nature* **2019**, *573*, 408−411.

(6) Kandasamy, N. K.; Tseng, K. J.; Boon-Hee, S. Virtual storage capacity using demand response management to overcome intermittency of solar PV generation. *IET Renew. Power Gener.* **2017**, *11*, 1741−1748.

(7) Ren, G.; Wan, J.; Liu, J.; Yu, D.; Söder, L. Analysis of wind power intermittency based on historical wind power data. *Energy* **2018**, *150*, 482−492.

(8) Amri, R.; Rezoug, T. Numerical study of liquid propellants combustion for space applications. *Acta Astronaut* **2011**, *69*, 485−498.

(9) Gambini, M.; Stilo, T.; Vellini, M. Hydrogen storage systems for fuel cells: Comparison between high and low-temperature metal hydrides. *Int. J. Hydrogen Energy* **2019**, *44*, 15118−15134.

(10) Manoharan, Y.; Hosseini, S. E.; Butler, B.; Alzhahrani, H.; Senior, B. T. F.; Ashuri, T.; Krohn, J. Hydrogen fuel cell vehicles; current status and future prospect. *Appl. Sci.* **2019**, *9*, 2296.

(11) Müller, K.; Arlt, W. Status and development in hydrogen transport and storage for energy applications. *Energy Technol.* **2013**, *1*, 501−511.

(12) Herbrig, K.; Röntzsch, L.; Pohlmann, C.; Weißgärber, T.; Kieback, B. Hydrogen storage systems based on hydride−graphite composites: computer simulation and experimental validation. *Int. J. Hydrogen Energy* **2013**, *38*, 7026−7036.

(13) Jiang, Z.; Pan, Q.; Xu, J.; Fang, T. Current situation and prospect of hydrogen storage technology with new organic liquid. *Int. J. Hydrogen Energy* **2014**, *39*, 17442−17451.

(14) Jean, P. Materials for Hydrogen Storage: Past, Present, and Future. *J. Phys. Chem. Lett.* **2011**, *2*, 206−211.
(15) Garrier, S.; Delhomme, B.; De Rango, P.; Marty, P.; Fruchart, D.; Miraglia, S. A new MgH_2 tank concept using a phase-change material to store the heat of reaction. *Int. J. Hydrogen Energy* **2013**, *38*, 9766−9771.
(16) Gambini, M.; Stilo, T.; Vellini, M. Selection of metal hydrides for a thermal energy storage device to support low-temperature concentrating solar power plants. *Int. J. Hydrogen Energy* **2020**, *45*, 28404−28425.
(17) Askri, F.; Jemni, A.; Nasrallah, S. B. Study of two-dimensional and dynamic heat and mass transfer in a metal−hydrogen reactor. *Int. J. Hydrogen Energy* **2003**, *28*, 537−557.
(18) Nogita, K.; Tran, X. Q.; Yamamoto, T.; Tanaka, E.; McDonald, S. D.; Gourlay, C. M.; Yasuda, K.; Matsumura, S. Evidence of the hydrogen release mechanism in bulk MgH2. *Sci. Rep.* **2015**, *5*, 8450.
(19) Zhou, C.; Peng, Y.; Zhang, Q. Growth kinetics of MgH_2 nanocrystallites prepared by ball milling. *J. Mater. Sci. Technol.* **2020**, *50*, 178−183.
(20) Chaise, A.; De Rango, P.; Marty, P.; Fruchart, D. Experimental and numerical study of a magnesium hydride tank. *Int. J. Hydrogen Energy* **2010**, *35*, 6311−6322.
(21) Delhomme, B.; de Rango, P.; Marty, P.; Bacia, M.; Zawilski, B.; Raufast, C.; Miraglia, S.; Fruchart, D. Large scale magnesium hydride tank coupled with an external heat source. *Int. J. Hydrogen Energy* **2012**, *37*, 9103−9111.
(22) Lutz, M.; Linder, M.; Bürger, I. High capacity, low pressure hydrogen storage based on magnesium hydride and thermochemical heat storage: Experimental proof of concept. *Appl. Energy* **2020**, *271*, No. 115226.
(23) Chaise, A.; Marty, P.; de Rango, P.; Fruchart, D. A simple criterion for estimating the effect of pressure gradients during hydrogen absorption in a hydride reactor. *Int. J. Heat Mass Transfer* **2009**, *52*, 4564−4572.
(24) Shen, D.; Zhao, C. Y. Thermal analysis of exothermic process in a magnesium hydride reactor with porous metals. *Chem. Eng. Sci.* **2013**, *98*, 273−281.
(25) Gi, H.; Shinzato, K.; Balgis, R.; Ogi, T.; Sadakane, M.; Wang, Y.; Isobe, S.; Miyaoka, H.; Ichikawa, T. Effective Factor on Catalysis of Niobium Oxide for Magnesium. *ACS Omega* **2020**, *5*, 21906−21912.
(26) Dong, D.; Humphries, T. D.; Sheooard, D. A.; Stansby, B.; Paskevicius, M.; Dornheim, M.; Buckley, C. E. Thermal optimisation of metal hydride reactors for thermal energy storage applications. *Sustainable Energy Fuels* **2017**, *1*, 1820−1829.
(27) Poupin, L.; Humphries, T. D.; Paskevicius, M.; Buckley, C. E. A thermal energy Sstorage prototype using sodium magnesium hydride. *Sustainable Energy Fuels* **2019**, *3*, 985−995.
(28) Zamengo, M.; Ryu, J.; Kato, Y. Thermochemical performance of magnesium hydroxide expanded graphite pellets for chemical heat pump. *Appl. Therm. Eng.* **2014**, *64*, 339−347.
(29) Bao, Z. Performance investigation and optimization of metal hydride reactors for high temperature thermochemical heat storage. *Int. J. Hydrogen Energy* **2015**, *40*, 5664−5676.
(30) Feng, P.; Zhu, L.; Zhang, Y.; Yang, F. S.; Wu, Z.; Zhang, Z. X. Optimum output temperature setting and an improved bed structure of metal hydride hydrogen storage reactor for thermal energy storage. *Int. J. Hydrogen Energy* **2019**, *44*, 19313−19325.
(31) Bogdanovic, B.; Bohmhammel, K.; Christ, B.; Reiser, A.; Schlichte, K.; Vehlen, R.; Wolf, U. Thermodynamic investigation of the magnesiumehydrogen system. *J. Alloys Compd.* **1999**, *282*, 84e92.
(32) Bao, Z.; Yang, F.; Wu, Z.; Cao, X.; Zhang, Z. Simulation studies on heat and mass transfer in high-temperature magnesium hydride reactors. *Appl. Energy* **2013**, *112*, 1181−1189.
(33) Gkanas, E. I.; Makridis, S. S. Effective thermal management of a cylindrical MgH_2 tank including thermal coupling with an operating SOFC and the usage of extended surfaces during the dehydrogenation process. *Int. J. Hydrogen Energy* **2016**, *41*, 5693−5708.
(34) Wu, Z.; Yang, F.; Zhu, L.; Feng, P.; Zhang, Z.; Wang, Y. Improvement in hydrogen desorption performances of magnesium based metal hydride reactor by incorporating helical coil heat exchanger. *Int. J. Hydrogen Energy* **2016**, *41*, 16108−16121.
(35) Bhouri, M.; Bürger, I. Numerical investigation of H2 absorption in an adiabatic high-temperature metal hydride reactor based on thermochemical heat storage: MgH_2 and $Mg(OH)_2$ as reference materials. *Int. J. Hydrogen Energy* **2017**, *42*, 16632−16644.
(36) Chung, C. A.; Lin, C. S. Prediction of hydrogen desorption performance of Mg_2Ni hydride reactors. *Int. J. Hydrogen Energy* **2009**, *34*, 9409−9423.
(37) Reiser, A.; Bogdanović, B.; Schlichte, K. The application of Mg-based metal-hydrides as heat energy storage systems. *Int. J. Hydrogen Energy* **2000**, *25*, 425−430.
(38) Baum, Z. J.; Diaz, L. L.; Konovalova, T.; Zhou, Q. Materials Research Directions Toward a Green Hydrogen Economy: A Review. *ACS Omega* **2022**, *7*, 32908−32935.

https://doi.org/10.1021/acsomega.2c03484
ACS Omega 2023, 8, 4586−4596